Resonance in fast-wave amplitude in the periphery of cylindrical plasmas and application to edge losses of wave heating power in tokamaks

R. J. Perkins, J. C. Hosea, N. Bertelli, G. Taylor, and J. R. Wilson

Citation: Physics of Plasmas **23**, 070702 (2016); doi: 10.1063/1.4954899
View online: http://dx.doi.org/10.1063/1.4954899
View Table of Contents: http://scitation.aip.org/content/aip/journal/pop/23/7?ver=pdfcov
Published by the AIP Publishing

Resonance in fast-wave amplitude in the periphery of cylindrical plasmas and application to edge losses of wave heating power in tokamaks

R. J. Perkins, J. C. Hosea, N. Bertelli, G. Taylor, and J. R. Wilson
Princeton Plasma Physics Laboratory, Princeton, New Jersey 08540, USA

(Received 22 March 2016; accepted 15 June 2016; published online 14 July 2016)

Heating magnetically confined plasmas using waves in the ion-cyclotron range of frequencies typically requires coupling these waves over a steep density gradient. This process has produced an unexpected and deleterious phenomenon on the National Spherical Torus eXperiment (NSTX): a prompt loss of wave power along magnetic field lines in front of the antenna to the divertor. Understanding this loss may be key to achieving effective heating and expanding the operational space of NSTX-Upgrade. Here, we propose that a new type of mode, which conducts a significant fraction of the total wave power in the low-density peripheral plasma, is driving these losses. We demonstrate the existence of such modes, which are distinct from surface modes and coaxial modes, in a cylindrical cold-plasma model when a half wavelength structure fits into the region outside the core plasma. The latter condition generalizes the previous hypothesis regarding the occurrence of the edge losses and may explain why full-wave simulations predict these losses in some cases but not others. If valid, this condition implies that outer gap control is a potential strategy for mitigating the losses in NSTX-Upgrade in addition to raising the magnetic field or influencing the edge density. *Published by AIP Publishing*. [http://dx.doi.org/10.1063/1.4954899]

Plasma-heating systems based on waves in the ion cyclotron range of frequencies (ICRF) are a leading candidate for heating burning plasmas due to proven wave physics in the core plasma and readily available high-power sources in this frequency range. The key challenge is coupling these waves across a steep density profile that can rise from below $10^{17}\,m^{-3}$ at the launching antenna near the outer edge to intermediate values of the order of $10^{18}\,m^{-3}$ in the scrape-off layer (SOL), and then to values of order $10^{19}\,m^{-3}$ as one enters the core. Over this gradient, ICRF waves typically transition from being radially cutoff at the antenna to fully propagating somewhere in the SOL. This transition is critical in high-harmonic fast-wave (HHFW) heating on the National Spherical Torus eXperiment (NSTX), where up to 60% of the coupled HHFW power is hypothesized to be lost to waves propagating in the SOL but never penetrating the core.[1] Full-wave simulations of NSTX using the AORSA code,[2] with the solution domain extended to include the SOL,[3] show that the RF electric field grows large in the SOL when the density at the antenna exceeds the right-hand cutoff density.[3,4] However, interpretation of the AORSA results is complicated by vessel and magnetic geometry,[5] and the fundamental reason for these losses was not fully understood. This limits our ability to mitigate the losses, which in turn limits the operational scenarios available to the NSTX program. It also limits predictive capability regarding the potential impact of such losses on future fusion experiments such as the multi-billion dollar ITER project.[6]

We use a cylindrical cold-plasma model to demonstrate a unique class of fast-wave modes that (1) conducts significant wave power in the low-density peripheral plasma and (2) constitutes a large fraction of the total antenna loading. Such modes are strong candidates for explaining the SOL losses observed on NSTX and for explaining why AORSA computes large amplitude RF fields in the SOL in some scenarios but not others. We refer to these modes as annulus resonances due to their enhanced amplitude and unique radial distribution of wave power. They are resonances of a radially bounded system, not to be confused with the unbounded wave resonance condition $k \to \infty$. Annulus resonances occur when a half-wavelength radial structure fits between the core plasma and vessel wall and demonstrate how a small region of diffuse plasma can drastically alter the global solution. The model is based upon that in Refs. 7–9, where similar results regarding edge wave propagation were found for ion cyclotron waves (slow waves) below the ion cyclotron frequency.[9] The present results are for modes that are predominantly fast wave at frequencies well above the ion cyclotron frequency. The cylindrical model is computationally inexpensive and allows a detailed study of individual modes, which is the key feature that allows the identification of the annulus resonances.

The model geometry, shown in Fig. 1, consists of three radial regions: a core plasma, a lower-density annulus, and an outer vacuum region. The core extends to radius r_c with constant density n_c. The annulus extends from $r = r_c$ to r_a with constant density n_a. The vacuum region extends from $r = r_a$ up to a conducting wall of radius r_w. A uniform axial magnetic field is used throughout. The coarse step profile is partially justified in that NSTX H-mode discharges have a relatively short density length scale of 1–2 cm at the separatrix[10,11] whereas the perpendicular fast-wave wavelength in the SOL is typically larger, for instance, 26 cm for a nominal SOL density of $2 \times 10^{18}\,m^{-3}$ and 7.9 cm at a nominal separatrix density of $10^{19}\,m^{-3}$, both at current-drive phasing. This step profile does not resolve the lower hybrid resonance layer, but we do not anticipate this layer having a significant impact on the propagating fields.[12] The antenna is modelled

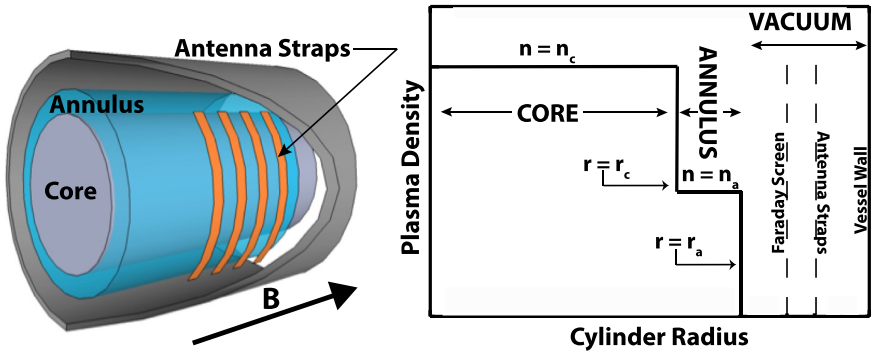

FIG. 1. Model geometry and radial density profile.

as current straps in the θ direction at $r = r_s$ with a Faraday screen at $r = r_F$. We chose NSTX-like parameters: $n_c = 5 \times 10^{19}\,\mathrm{m}^{-3}$, $f = 30\,\mathrm{MHz}$, $B = 0.32\,\mathrm{T}$ (approximate field at the edge for a 0.55 T on-axis field), $r_c = 0.515$ m, $r_a = 0.575$ m, $r_F = 0.600$ m, $r_s = 0.650$ m, and $r_w = 0.700$ m.

A "mode" refers to a global solution which satisfies the wave equation in each region and which is matched at interfaces. Modes assume the form $\tilde{E}_z(r, m, k_\parallel) = \tilde{E}_z(r)\exp(im\theta + ik_\parallel z - i\omega t)$, based on Fourier analysis in the axial and azimuthal directions. With $k_\parallel$ given, $k_\perp$ is fixed in each region by the cold-plasma dispersion, with the slow-wave and vacuum $k_\perp$ always cutoff. Radial RF field profiles are found by the method detailed in Ref. 13. Each region admits four independent solutions. In plasma, there are two fast-wave solutions and two (cutoff) slow-wave solutions; in vacuum there are exponentially decaying and growing E_z (transverse magnetic) and H_z (transverse electric) modes. Four boundary conditions are required at each interface: namely, continuity of E_z, H_z, E_ϕ, and H_ϕ. The twelve total coefficients can be reduced to four by the following: (i) continuity at the core-annulus interface specifies the four annulus coefficients in terms of the core coefficients, (ii) the fields must remain finite at $r = 0$, which requires setting two core coefficients to zero, and (iii) E_z must vanish at the Faraday screen and E_ϕ at the vessel wall, eliminating two vacuum coefficients. We are left with four coefficients α_i, with $i = 1$ the core fast wave, $i = 2$ the core slow mode, $i = 3$ the vacuum E_z mode that vanishes at the Faraday screen, and $i = 4$ the vacuum H_z mode whose E_ϕ component vanishes at the vessel wall. To formulate the final boundary condition, continuity at the annulus-vacuum interface, we form column vectors $(E_z, H_z, E_\phi, H_\phi)$ of the fields required for continuity. Let $\mathbf{v}_i$ be the column vector of form factors that, when multiplied by α_i, give the field components of that solution evaluated at $r = r_a$. For instance, $(E_z^{\mathrm{fast}}, H_z^{\mathrm{fast}}, E_\phi^{\mathrm{fast}}, H_\phi^{\mathrm{fast}})_{r=r_a} = \alpha_1\mathbf{v}_1$. Continuity at $r = r_a$ is then expressed as

$$\alpha_1\mathbf{v}_1 + \alpha_2\mathbf{v}_2 = \alpha_3\mathbf{v}_3 + \alpha_4\mathbf{v}_4 + \mathbf{So}, \tag{1}$$

where **So** is an inhomogeneous source term introduced by the antenna current whose exact form does not concern us here. In the absence of any antenna current ($\mathbf{So} = 0$), modes only exist when $\det(\mathbf{v}_1, \mathbf{v}_2, \mathbf{v}_3, \mathbf{v}_4) = 0$. Define the system dispersion function $F(k_\parallel) = \det(\mathbf{v}_1, \mathbf{v}_2, \mathbf{v}_3, \mathbf{v}_4)$ so that modes exist at the roots of $F(k_\parallel)$.

The coefficients α_i of modes excited by an antenna current ($\mathbf{So} \neq 0$) are given by Cramer's rule, e.g.,

$$\alpha_4 = \frac{\det(\mathbf{v}_1, \mathbf{v}_2, \mathbf{v}_3, \mathbf{So})}{\det(\mathbf{v}_1, \mathbf{v}_2, \mathbf{v}_3, \mathbf{v}_4)}, \tag{2}$$

and thus have simple poles at the $k_\parallel$ values of the modes. Therefore, upon inverse Fourier transform to find the total field,

$$E_\theta = \sum_m \int \tilde{E}_\theta(r, m, k_\parallel) J_{\mathrm{ant}}(m, k_\parallel) e^{im\theta + ik_\parallel z} dk_\parallel, \tag{3}$$

the integral reduces to a sum of residues, one for each mode. In Eq. (3), $J_{\mathrm{ant}}(m, k_\parallel)$ is the antenna spectral current density and $\tilde{E}_\theta$ is the azimuthal electric field per unit antenna spectral current density. The amplitude of each mode is thus given by two factors: (i) the amplitude of $J_{\mathrm{ant}}(m, k_\parallel)$ at the $k_\parallel$ of the mode and (ii) the size of the residue, which is proportional to $(dF(k_\parallel)/dk_\parallel)^{-1}$. We show that the annulus resonance is due to a near vanishing of $dF(k_\parallel)/dk_\parallel$, which is an important result, as $F(k_\parallel)$ is independent of antenna geometry.

The annulus resonances have enhanced amplitudes compared to other modes and carry significant power in the annulus region. Mode amplitude is measured by the total wave power P for the mode, calculated by integrating the axial Poynting flux over the cylinder cross-section. We express this as a loading resistance R such that $P = (1/2)RI_{\mathrm{ant}}^2$, with I_{ant} being the antenna current. The annulus resonances are the peaks in loading resistance in Fig. 2(a). The $k_\parallel$ of the peak depends on the annulus density and can be thus moved onto or off of an antenna spectral peak, consistent with the experimental observation that the NSTX SOL losses are strongly dependent on SOL density.[1] At high enough density, two resonances can appear, as shown by the $n_a = 1.0 \times 10^{19}\,\mathrm{m}^{-3}$ curve in Fig. 2(a). $m = 2$ was chosen for illustrative purposes; Fig. 2(a) is similar for other m. To study the loading curve without complications from any particular antenna spectrum, the calculations in Fig. 2 use a single-strap antenna, $J_{\mathrm{ant}}(z) = I_{\mathrm{ant}}\delta(z)$, which gives equal weight to all modes. The large modes at very low $k_\parallel$ are spurious coaxial modes discussed below. Figure 2(b) plots the partition of wave power among the different regions; the axial Poynting flux is integrated over the core, annulus, and vacuum cross-sections. Whereas most modes conduct nearly 100% of their wave power in the core, the annulus resonance conducts 47% in the core, 45% in the annulus, and 8% in the vacuum, while the coaxial mode conducts power entirely in the vacuum region. The term "annulus resonance" is rationalized by the sharp

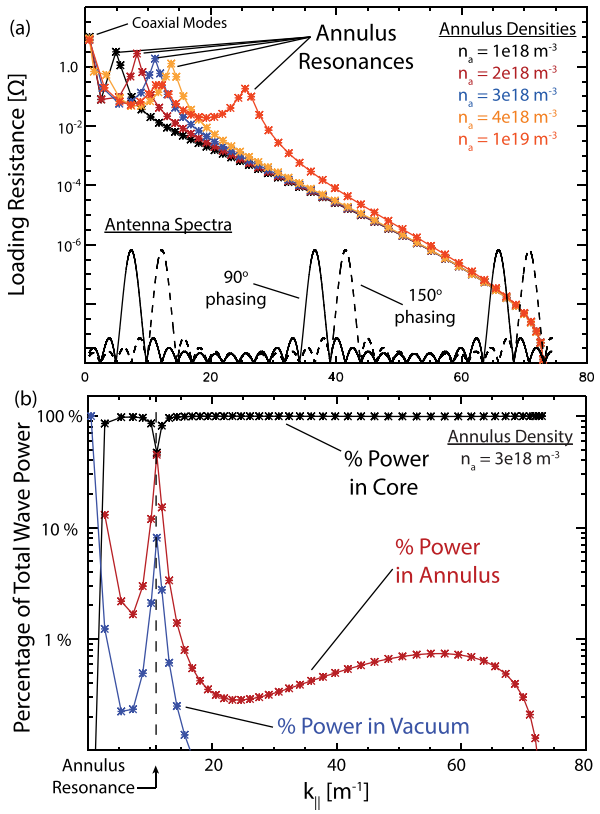

FIG. 2. (a) Loading resistance of $m = 2$ modes for various annulus densities n_a. Antenna spectra for model twelve-strap antenna with 21 cm inter-strap spacing and 90° and 150° phasing are plotted for reference. (b) Percentage of wave power conducted by each mode in the core (black), annulus (red), and vacuum (blue) regions for the $n_a = 3 \times 10^{18}\,\mathrm{m}^{-3}$ case of (a).

change in radial distribution of Poynting flux shown in this figure.

We note here that the model presently does not include absorption in the core and edge regions; wave power coupled from the antenna propagates axially without loss. Indeed, the mechanism converting HHFW power in the SOL to a divertor heat flux is not yet identified, but dissipation by far-field RF sheaths is a leading candidate[14] to be explored in upcoming HHFW experiments. Core absorption is the usual Landau damping and transit-time magnetic pumping. We presume that the high edge field amplitude of the annulus resonance will drive a high rate of edge absorption relative to core absorption once the proper SOL damping mechanism is identified and included, but this remains a crucial future step to verify.

The very low-$k_\parallel$ modes in Fig. 2(a) can be identified as coaxial modes,[15,16] low-$k_\parallel$ modes resembling the $m = 2$ TEM (transverse electromagnetic) modes found in the coaxial cable formed by replacing the plasma with a conductor. One such coaxial mode appears for every m except for $m = 0$, which has zero E_θ and does not couple to the antenna. Fig. 2(a) shows that the $k_\parallel$ of this mode is insensitive to the annulus density, and Fig. 2(b) shows that the fields are largely excluded from the plasma and are confined to the vacuum. Despite the enormous loading resistance, this mode is often considered spurious and removed from analysis.[15,17] The coaxial mode drives a large axial current sheet in the Faraday screen and cannot propagate without it. In this modal analysis, the Faraday screen boundary condition extends to $z = \pm\infty$ due to Fourier transformation in the z direction. With a Faraday screen of finite extent, it seems unlikely that the low-$k_\parallel$ coaxial modes could propagate axially beyond the screen. Regardless, the annulus resonance is distinct from coaxial modes in several regards. It is not a TEM mode, since it has a substantial H_z component. From Fig. 2(b), the wave fields do penetrate substantially into the core plasma, and the $k_\parallel$ value of the annulus resonance is sensitive to the annulus density. Nor does this mode meet the second criterion of Ref. 15, $k_r \approx 0$, in any region. Finally, coaxial modes do not appear for $m = 0$ but the annulus resonance does. Also, the annulus resonances are distinct from surface modes,[15,16] which would decay exponentially as one moves inward radially.

The annulus resonance occurs when a half wavelength in the radial direction fits into the combined annulus and vacuum regions. Figure 3 shows $E_\theta(r)$ for the two annulus resonances seen in the $n_a = 1.0 \times 10^{19}\,\mathrm{m}^{-3}$ case of Fig. 2(a). For the resonance at $k_\parallel = 25.5\,\mathrm{m}^{-1}$, E_θ undergoes

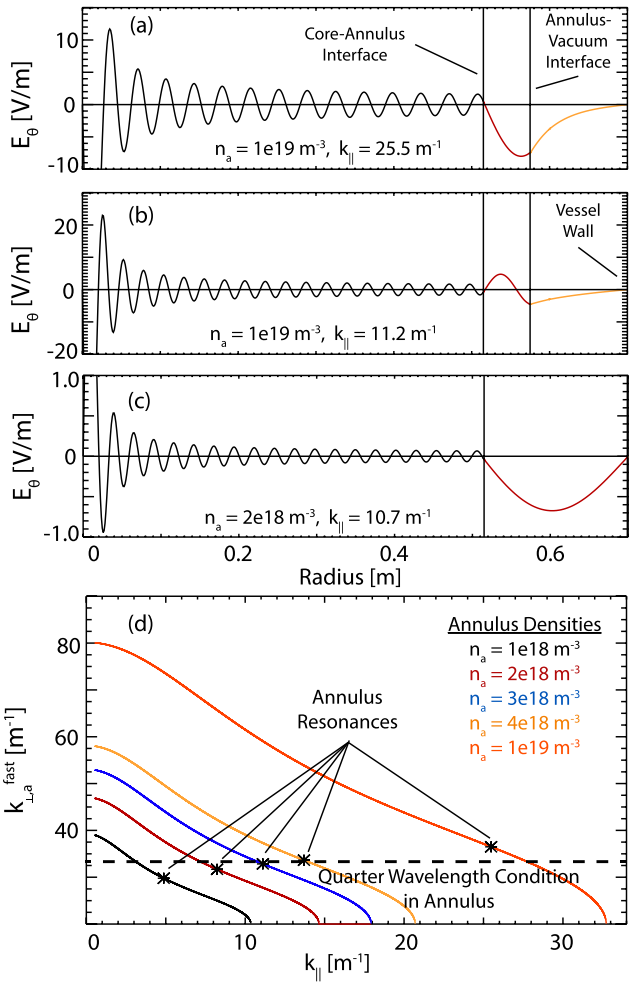

FIG. 3. (a) $E_\theta(r)$ for the annulus resonance at $k_\parallel = 25.5\,\mathrm{m}^{-1}$ for $n_a = 1.0 \times 10^{19}\,\mathrm{m}^{-3}$. (b) $E_\theta(r)$ for the annulus resonance at $k_\parallel = 11.2\,\mathrm{m}^{-1}$ for $n_a = 1.0 \times 10^{19}\,\mathrm{m}^{-3}$. (c) $E_\theta(r)$ for the annulus resonance at $k_\parallel = 10.7\,\mathrm{m}^{-1}$ for $n_a = 2.0 \times 10^{18}\,\mathrm{m}^{-3}$ under the special condition that the annulus outer radius extends to the wall, eliminating the vacuum region. (d) $k_\perp^{\mathrm{fast}}$ for the different annulus densities in Fig. 2(a), which changes very gradually with density even though $k_\parallel$ changes substantially. For reference, the dashed line is the $k_{\perp,a}^{\mathrm{fast}}$ value that gives a quarter wavelength in the annulus alone.

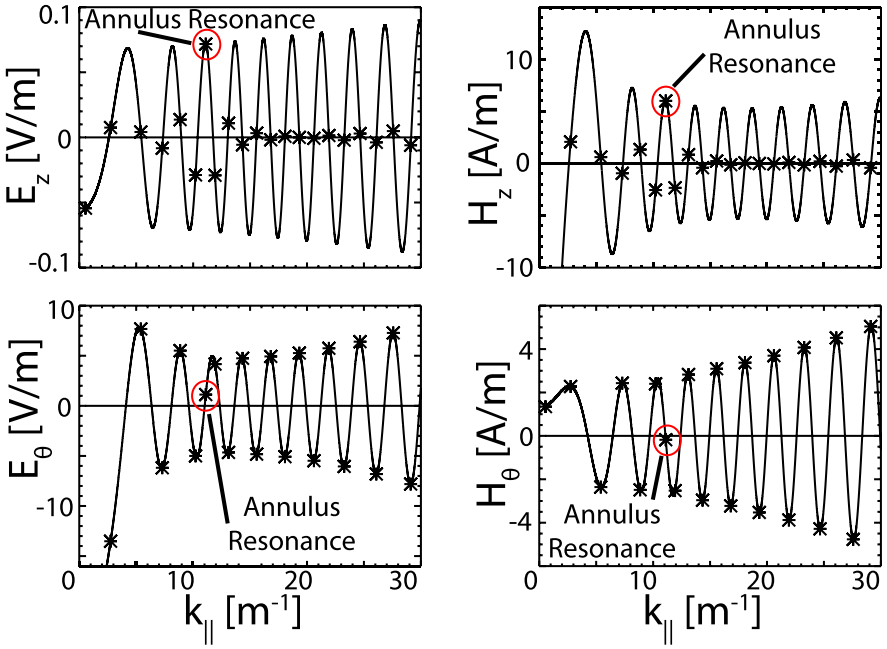

FIG. 4. Core fast-wave fields at $r = r_c$ as a function of $k_\parallel$ with mode locations indicated by stars. $m = 2$ and $n_a = 3.0 \times 10^{18}\,\mathrm{m}^{-3}$. The annulus resonance is 90° out of phase with other modes.

approximately one quarter of a cycle over the annulus (and one half cycle over the annulus plus vacuum regions), while the resonance at $k_\parallel = 11.2\,\mathrm{m}^{-1}$ undergoes approximately three quarters of a cycle over the annulus and one full cycle over the annulus plus vacuum. If the vacuum region is eliminated by extending the annulus radius r_a to the wall, as done in Fig. 3(c), then the half wavelength structure fills the entire annulus region. Figure 3(d) plots $k_{\perp,a}^{\mathrm{fast}}$ for each n_a used in Fig. 2(a) and indicates the locations of the annulus resonances. While the $k_\parallel$ of the annulus resonance changes strongly with n_a, $k_{\perp,a}^{\mathrm{fast}}$ changes only gradually. Changing the core density hardly alters the $k_\parallel$-value of the annulus resonance.

The half-radial-wavelength condition allows the RF fields from the annulus to match fields in the core in a unique fashion. Typical modes have a particular core fast-wave phase at the core-annulus interface; Fig. 4 plots the core fast-wave fields at $r = r_c$ as a function of $k_\parallel$, and most modes fall primarily at the peaks of H_ϕ and E_ϕ and the nodes of H_z and E_z. The E_θ and H_θ radial profiles for such modes typically contain an integral number of half wavelengths plus a quarter. The annulus resonance, however, occurs for a core fast-wave phase 90° out of phase with the other modes and falls at a node for H_ϕ and E_ϕ and a peak for H_z and E_z. It contains an integral number of half wavelengths in the core. The unique fast-wave phase of the annulus resonance at the core-annulus interface explains the high loading resistance of this mode when the core fast-wave fields are propagated to the annulus-vacuum interface. This is done by solving for the four annulus coefficients that match a pure core fast wave and evaluating the fields at $r = r_a$; these fields are precisely the components of $\mathbf{v}_1$. Figure 5 shows that the annulus resonance falls at maxima in H_ϕ and E_ϕ and very close to the maxima in H_z and E_z at

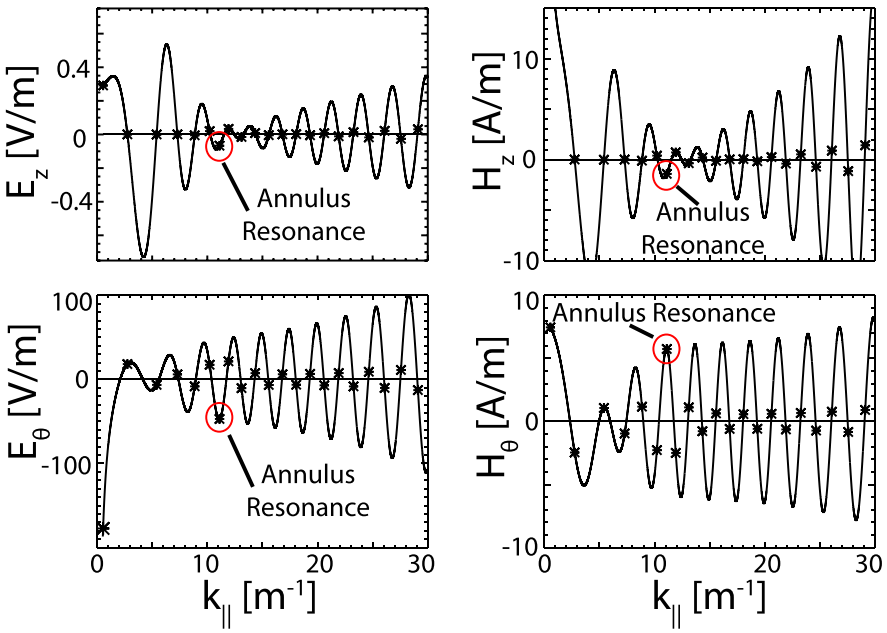

FIG. 5. Similar to Fig. 4 but evaluated at $r = r_a$. The annulus resonance lies near a local maxima for all field components.

TABLE I. $n_{e,\pi}$ for the cases analyzed in Ref. 5. $n_\phi = k_\parallel/R$ is the toroidal mode number with R being the major radius. ΔR is the midplane distance from the separatrix to the vessel wall. $n_{e,\mathrm{LCFS}}$ is the density at the separatrix, for reference.

Machine	n_ϕ	F (MHz)	B_T (T)	ΔR (cm)	$n_{e,\pi}$ (10^{18} m^{-3})	$n_{e,\mathrm{LCFS}}$ (10^{18} m^{-3})
NSTX	12	30	0.55	18	1.4	8.0
NSTX	21	30	0.55	18	2.9	8.0
DIII-D	15	90	1.85	25	1.3	10
DIII-D	15	60	1.85	25	2.2	10
EAST	12	27	1.95	9.3	22	2.5
C-Mod	10	80	5.41	4.5	92	19

$r = r_a$. Recall that the mode amplitude is inversely proportional to $dF/dk_\parallel$, which is dominated by the term $\det(d\mathbf{v}_1/dk_\parallel, \mathbf{v}_2, \mathbf{v}_3, \mathbf{v}_4)$, because $\mathbf{v}_1$ changes on the scale of the core fast-wave (since the core-slow-wave dependence is cutoff and exponentially growing, $d\mathbf{v}_2/dk_\parallel = |k_{\perp,c}^{\mathrm{slow}}|\mathbf{v}_2$, and $\det(\mathbf{v}_1, d\mathbf{v}_2/dk_\parallel, \mathbf{v}_3, \mathbf{v}_4) \approx 0$ when evaluated at a mode). From Fig. 5, $d\mathbf{v}_1/dk_\parallel$ is small for the annulus resonance because it lies very near a local maximum for all fields, giving a large loading resistance.

The half-radial-wavelength condition for the annulus resonance refines the original hypothesis that SOL losses occur when the density at the antenna exceeds the right-hand cutoff density. This could explain why AORSA calculates large RF field amplitudes in the SOL for NSTX and DIII-D for certain SOL densities but not for Alcator C-Mod and EAST even when the antenna density exceeds the cutoff.[5] In these simulations, the SOL density profile is nearly flat from the separatrix out to the wall.[4] With no vacuum region, the annulus resonances occur when a half-wavelength occurs in the annulus (as in Fig. 3(c)): $k_\perp^{\mathrm{fast}}\Delta R \approx \pi$, with ΔR the width of the annulus. Table I shows the critical density, $n_{e,\pi}$, above which annulus resonance would occur in the model, for each case in Ref. 5. $n_{e,\pi}$ is similar for the NSTX and DIII-D cases; the measured SOL density in previous NSTX HHFW experiments routinely exceeds these values. For EAST and C-Mod, where AORSA does not predict an increase in SOL field amplitude, the required $n_{e,\pi}$ is far too large to be achieved in the SOL. While speculative, Table I indicates the potential role of the SOL and vessel geometry so that outer gap control may be another strategy for mitigating the SOL losses in NSTX-Upgrade in addition to raising the magnetic field[1,4] and influencing the SOL density with lithium conditioning.[18] Future modeling work will study the half-wavelength condition in three-dimensional reconstructions of the wave fields not only for the mean SOL density profile but also for the high-density excursions, which are known to be substantial.[10,11]

This work was supported by DOE Contract No. DE-AC02-09CH11466. The digital data for this paper can be found in http://arks.princeton.edu/ark:/88435/dsp018p58pg29j. We gratefully acknowledge R. I. Pinsker and S. J. Zweben for useful discussions and S. M. Kaye and P. T. Bonoli for critically reading the manuscript.

[1]J. Hosea, R. E. Bell, B. P. LeBlanc, C. K. Phillips, G. Taylor, E. Valeo, J. R. Wilson, E. F. Jaeger, P. M. Ryan, J. Wilgen, H. Yuh, F. Levinton, S. Sabbagh, K. Tritz, J. Parker, P. T. Bonoli, R. Harvey, and NSTX Team, "High harmonic fast wave heating efficiency enhancement and current drive at longer wavelength on the National Spherical Torus Experimental," Phys. Plasmas **15**(5), 056104 (2008).
[2]E. F. Jaeger, L. A. Berry, E. F. DAzevedo, R. F. Barrett, S. D. Ahern, D. W. Swain, D. B. Batchelor, R. W. Harvey, J. R. Myra, D. A. DIppolito, C. K. Phillips, E. Valeo, D. N. Smithe, P. T. Bonoli, J. C. Wright, and M. Choi, "Simulation of high-power electromagnetic wave heating in the ITER burning plasma," Phys. Plasmas **15**(7), 072513 (2008).
[3]D. L. Green, L. A. Berry, G. Chen, P. M. Ryan, J. M. Canik, and E. F. Jaeger, "Predicting high harmonic ion cyclotron heating efficiency in tokamak plasmas," Phys. Rev. Lett. **107**, 145001 (2011).
[4]N. Bertelli, E. Jaeger, J. Hosea, C. Phillips, L. Berry, S. Gerhardt, D. Green, B. LeBlanc, R. Perkins, P. Ryan, G. Taylor, E. Valeo, and J. Wilson, "Full wave simulations of fast wave heating losses in the scrape-off layer of NSTX and NSTX-U," Nucl. Fusion **54**(8), 083004 (2014).
[5]N. Bertelli, E. Jaeger, J. Hosea, C. Phillips, L. Berry, P. Bonoli, S. Gerhardt, D. Green, B. LeBlanc, R. Perkins, C. Qin, R. Pinsker, R. Prater, P. Ryan, G. Taylor, E. Valeo, J. Wilson, J. Wright, and X. Zhang, "Full wave simulations of fast wave efficiency and power losses in the scrape-off layer of tokamak plasmas in mid/high harmonic and minority heating regimes," Nucl. Fusion **56**(1), 016019 (2016).
[6]N. Holtkamp, "An overview of the ITER project," Fusion Eng. Des. **82**(514), 427–434 (2007).
[7]J. C. Hosea and R. M. Sinclair, "Dominant influence of electron inertia on ion cyclotron-wave generation in plasma," Phys. Rev. Lett. **23**, 3–7 (1969).
[8]J. C. Hosea and R. M. Sinclair, "Ion cyclotron wave generation in the Model C Stellarator," Phys. Fluids **13**(3), 701–711 (1970).
[9]J. C. Hosea and R. M. Sinclair, "Effect of the plasma density profile on ion cyclotron wave generation," Phys. Fluids **16**(8), 1268–1272 (1973).
[10]S. J. Zweben, R. R. Myra, W. M. Davis, D. A. D'Ippolito, T. K. Gray, S. M. Kaye, B. P. LeBlanc, R. J. Maqueda, D. A. Russell, D. P. Stotler, and NSTX-U Team, "Blob structure and motion in the edge of NSTX," Plasma Phys. Controlled Fusion **58**, 044007 (2016).
[11]J. A. Boedo, J. R. Myra, S. Zweben, R. Maingi, R. J. Maqueda, V. A. Soukhanovskii, J. W. Ahn, J. Canik, N. Crocker, D. A. D'Ippolito, R. Bell, H. Kugel, B. Leblanc, L. A. Roquemore, D. L. Rudakov, and NSTX Team, "Edge transport studies in the edge and scrape-off layer of the National Spherical Torus Experiment with Langmuir probes," Phys. Plasmas **21**(4), 042309 (2014).
[12]L. Lu, K. Crombé, D. V. Eester, L. Colas, J. Jacquot, and S. Heuraux, "Ion cyclotron wave coupling in the magnetized plasma edge of tokamaks: Impact of a finite, inhomogeneous density inside the antenna box," Plasma Phys. Controlled Fusion **58**, 055001 (2016).
[13]W. P. Allis, S. J. Buchsbaum, and A. Bers, *Waves in Anisotropic Plasmas* (The MIT Press, 1963), Vol. 1.
[14]R. J. Perkins, J. C. Hosea, M. A. Jaworski, J.-W. Ahn, A. Diallo, R. E. Bell, N. Bertelli, S. Gerhardt, T. K. Gray, G. J. Kramer, B. P. LeBlanc, A. McLean, C. K. Phillips, M. Podest, L. Roquemore, S. Sabbagh, G. Taylor, and J. R. Wilson, "The contribution of radio-frequency rectification to field-aligned losses of high-harmonic fast wave power to the divertor in the National Spherical Torus eXperiment," Phys. Plasmas **22**(4), 042506 (2015).
[15]A. Messiaen, R. Koch, V. Bhatnagar, P. Vandenplas, and R. Weynants, "Analysis of the plasma edge radiation by ICRH antenna," in *Proceedings of the 4th International Symposium on Heating in Toroidal Plasmas, Rome, 1984*, Vol. 1, pp. 315–329.
[16]R. Pinsker and P. Colestock, "Effect of surface modes on coupling to fast waves in the lower hybrid range of frequencies," Nucl. Fusion **32**(10), 1789 (1992).
[17]S. Pècoul, S. Heuraux, R. Koch, and G. Leclert, "Numerical modeling of the coupling of an ICRH antenna with a plasma with self-consistent antenna currents," Comput. Phys. Commun. **146**(2), 166–187 (2002).
[18]G. Taylor, R. E. Bell, J. C. Hosea, B. P. LeBlanc, C. K. Phillips, M. Podestà, E. J. Valeo, J. R. Wilson, J.-W. Ahn, G. Chen, D. L. Green, E. F. Jaeger, R. Maingi, P. M. Ryan, J. B. Wilgen, W. W. Heidbrink, D. Liu, P. T. Bonoli, T. Brecht, M. Choi, and R. W. Harvey, "Advances in high-harmonic fast wave physics in the National Spherical Torus Experiment," Phys. Plasmas **17**(5), 056114 (2010).